ACS APPLIED MATERIALS & INTERFACES

Research Article

www.acsami.org

Chemically Exfoliated MoS_2 Nanosheets as an Efficient Catalyst for Reduction Reactions in the Aqueous Phase

Laura Guardia,* Juan I. Paredes, José M. Munuera, Silvia Villar-Rodil, Miguel Ayán-Varela, Amelia Martínez-Alonso, and Juan M. D. Tascón

Instituto Nacional del Carbón, INCAR-CSIC, Apartado 73, 33080 Oviedo, Spain

Supporting Information

ABSTRACT: Chemically exfoliated MoS_2 (ce-MoS_2) nanosheets that incorporate a large fraction of metallic 1T phase have been recently shown to possess a high electrocatalytic activity in the hydrogen evolution reaction, but the potential of this two-dimensional material as a catalyst has otherwise remained mostly uncharted. Here, we demonstrate that ce-MoS_2 nanosheets are efficient catalysts for a number of model reduction reactions (namely, those of 4-nitrophenol, 4-nitroaniline, methyl orange, and $[Fe(CN)_6]^{3-}$) carried out in aqueous medium using $NaBH_4$ as a reductant. The performance of the nanosheets in these reactions is found to be comparable to that of many noble metal-based catalysts. The possible reaction pathways involving ce-MoS_2 as a catalyst are also discussed and investigated. Overall, the present results expand the scope of this two-dimensional material as a competitive, inexpensive, and earth-abundant catalyst.

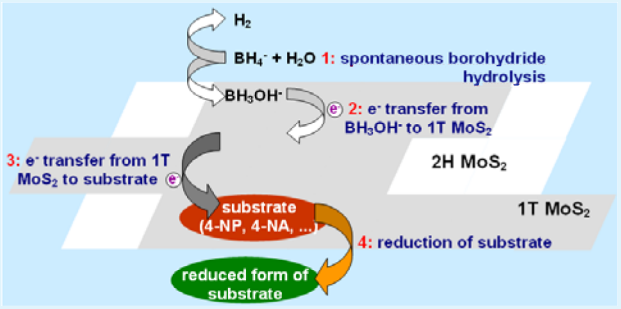

KEYWORDS: *MoS_2, two-dimensional material, transition metal dichalcogenides (TMDs), reduction reaction, heterogeneous catalysis*

1. INTRODUCTION

Catalysts are a central component of modern science and technology, playing a pivotal role in such diverse areas as the synthesis of oil-derived products as well as pharmaceutical compounds and other fine chemicals, the operation of fuel cells, or the conversion of harmful car exhaust emissions into less toxic gases, to name but some relevant examples.[1] For many of these processes, encompassing both homogeneous and heterogeneous catalysis, the most efficient catalysts are frequently based on noble metals, but their scarcity and high cost has driven a search for more cost-effective alternatives that make use of earth-abundant elements.[2−5]

Transition metal dichalcogenides (TMDs) with a lamellar structure, such as MoS_2, WSe_2, or VS_2, have received in recent years renewed interest from the scientific community in relation to the development of novel two-dimensional (2D) materials beyond graphene.[6−8] Similar to the case of the latter, many single- or few-layered TMDs exhibit a host of attractive physical properties that differ from those of their bulk counterpart, which has opened up the prospect of technological application for such 2D materials in, e.g., electronics, photonics, sensing, biomedicine, or photocatalysis.[7−9] In the context of catalysis, having single layers of TMDs (or of any other lamellar material) is potentially advantageous compared to their bulk form because the surface area available for interaction with substrates is maximized, as long as the newly exposed surface is catalytically active.[10,11]

As a prominent member of the TMD family, MoS_2 has long been known to be an efficient hydrodesulfurization catalyst,[12] and more recently it was demonstrated to exhibit a high catalytic activity toward the hydrogen evolution reaction (HER) as well.[13−15] Experimental and theoretical studies have determined that the catalytic activity of the thermodynamically stable 2H polymorph of MoS_2 is associated with metallic edges, whereas its semiconducting basal plane is catalytically inert.[13,14] As a result, a great deal of work has aimed at nanostructuring this material so as to maximize the fraction of exposed edge sites and thus its catalytic activity.[15] On the other hand, a new perspective on the catalysis of MoS_2 and related TMDs has been very recently disclosed by the observation that single-layered chemically exfoliated MoS_2 (ce-MoS_2) nanosheets, prepared via a lithium intercalation route, are excellent catalysts for the HER.[16,17] Such behavior was attributed to the conversion of the 2H (trigonal prismatic) phase of MoS_2 to the intrinsically metallic, although metastable, 1T (octahedral) phase during the chemical exfoliation step.

However, with the exception of HER, the catalytic activity of ce-MoS_2 nanosheets has not been explored for the most part, and therefore it is currently unknown whether such activity is limited to HER or encompasses other types of reaction. Here, we show that the latter is the case by investigating the performance of ce-MoS_2 as a catalyst in several model reduction reactions carried out in the aqueous phase at room temperature and using $NaBH_4$ as the reductant. The results indicate that the

Received: October 8, 2014
Accepted: November 18, 2014
Published: November 18, 2014

activity of ce-MoS_2 nanosheets is comparable to that of many noble metal nanoparticle-based catalysts typically used for the same reactions, thereby suggesting that this 2D material could be put to good use in a host of catalytic reactions as an inexpensive, earth-abundant alternative to the mentioned metals.

2. EXPERIMENTAL SECTION

2.1. Materials. MoS_2 powder, hexane, 1.6 M *n*-butyllithium solution in hexane, 4-nitrophenol, 4-nitroaniline, methyl orange, $K_3[Fe(CN)_6]$, and $NaBH_4$ were obtained from Sigma-Aldrich and used as received. Dialysis membranes (14 000 Da molecular weight cutoff) made from cellulose ester were purchased from Sigma-Aldrich. Alumina membrane filters 47 mm in diameter and 0.2 μm of pore size were acquired from Whatman.

2.2. Instrumentation. UV−vis absorption spectroscopy was carried out with a double-beam Heλios α spectrophotometer, from Thermo Spectronics. X-ray photoelectron spectroscopy (XPS) was accomplished on a SPECS system at a pressure of 10^{-7} Pa with a nonmonochromatic Mg Kα X-ray source operated at a power of 100 W. Raman spectra were recorded on a Horiba Jobin Yvon LabRam apparatus using a laser excitation wavelength of 532 nm. To avoid damaging/altering the MoS_2 specimens, the incident laser power was kept at a low value (~0.5 mW). Samples for both XPS and Raman spectroscopy were prepared in the form of thin free-standing films through vacuum filtration of the corresponding aqueous suspension through alumina membrane filters. Atomic force microscopy (AFM) imaging of the ce-MoS_2 nanosheets was performed with a Nanoscope IIIa Multimode apparatus (Veeco Instruments) in the tapping mode of operation. Rectangular silicon cantilevers with nominal spring constant of about 40 N m^{-1} and resonance frequency in the 250−300 kHz range were employed. Samples for AFM were prepared by drop-casting dilute ce-MoS_2 suspensions (~0.01−0.02 mg mL^{-1}) onto mica substrates and allowing them to dry under ambient conditions. Field emission scanning electron microscopy (FE-SEM) images were obtained with a Quanta FEG 650 instrument, from FEI Company. Samples for FE-SEM were prepared by drop-casting dilute ce-MoS_2 suspensions (~0.01−0.02 mg mL^{-1}) onto preheated (~50−60 °C) highly oriented pyrolytic graphite (HOPG) substrates, which were then allowed to dry under ambient conditions.

2.3. Preparation of ce-MoS_2 Nanosheets. In a typical preparation procedure,[18,19] 3 mL of 1.6 M *n*-butyllithium solution in hexane were poured into 300 mg of MoS_2 powder, and the mixture was left to stand under static conditions at room temperature for 48 h in an argon-filled glovebox. The resulting lithium-intercalated product (Li_xMoS_2) was rinsed with 60 mL of hexane to remove unreacted *n*-butyllithium and its organic residues. Immediately after this, the intercalated MoS_2 was dispersed in Milli-Q water and exfoliated through bath sonication (Selecta Ultrasons system, 40 kHz, power ~20 W L^{-1}) for 1 h, leading to a stable aqueous suspension of ce-MoS_2 nanosheets. Excess lithium was removed from the dispersion by dialysis against Milli-Q water. The suspension concentration was estimated by means of UV−vis absorption spectroscopy using the Lambert−Beer law that relates the measured absorbance at a given wavelength to the suspension concentration by the formula $A/l = \alpha C$, where A is the absorbance, l is the optical path length, α is the extinction coefficient, and C is the suspension concentration. α was determined from a calibration curve obtained by measuring the absorbance of a starting ce-MoS_2 dispersion that was then consecutively diluted and measured. The concentration of the starting dispersion was gauged by weighing a free-standing film that was obtained through vacuum filtration of a known volume of the dispersion. The values of α were measured to be 11952, 11285, and 5045 L m^{-1} g^{-1} at wavelengths of 257, 307, and 450 nm, respectively. The concentration of the as-prepared aqueous ce-MoS_2 suspensions was seen to differ somewhat from batch to batch, but it was between 0.3 and 0.5 mg mL^{-1} in all cases.

2.4. Hydrothermal Conversion of 1T ce-MoS_2 to 2H ce-MoS_2 Nanosheets. Transformation of the ce-MoS_2 nanosheets from their dominant 1T phase generated during the lithium intercalation process to the 2H phase was accomplished by means of hydrothermal treatment. To this end, 20 mL of 1T ce-MoS_2 suspension (0.05 mg mL^{-1}) was transferred to a Teflon-lined autoclave (capacity: 50 mL) and heated at 200 °C for 4 h. After being allowed to cool down to room temperature, the product was recovered from the autoclave as a homogeneous dispersion and used without further processing. The main requirement for the attainment of stable homogeneous suspensions of 2H ce-MoS_2 by this method was to work at moderate to low concentrations of MoS_2 (<0.1 mg mL^{-1}). Otherwise, the hydrothermally converted product was obtained as a precipitate that could not be redispersed in water.

2.5. Preparation of Nitrogen-Doped and Undoped Reduced Graphene Oxide Nanosheets. Graphene oxide nanosheets in aqueous dispersion were prepared following methods reported in the literature.[20] To obtain a suspension of undoped reduced nanosheets, 20 mL of the starting, as-prepared graphene oxide dispersion (0.1 mg mL^{-1}, pH ~ 4) were transferred to a Teflon-lined autoclave with a total capacity of 50 mL and heated at 180 °C for 6 h.[21,22] For the preparation of nitrogen-doped reduced nanosheets, the same procedure was followed with the exception that 25% ammonia solution was added to the graphene oxide dispersion (2 μL per mL of suspension) prior to the hydrothermal treatment.[23]

2.6. Testing of the Catalytic Behavior of ce-MoS_2 Nanosheets. *Reduction of 4-Nitrophenol (4-NP).* In a typical reduction experiment a given amount of ce-MoS_2 was mixed with 4-NP solution, and then $NaBH_4$ solution was added to trigger the reduction reaction. Specifically, for an initial 4-NP concentration of 0.12 mM the $NaBH_4$ concentration employed was 72 mM, i.e., the 4-NP:$NaBH_4$ molar ratio was 1:600. The reaction progress was monitored by measuring the absorbance of the peak located at 400 nm which is characteristic of the 4-nitrophenolate anion. The excess amount of $NaBH_4$ used ensured that its concentration could be considered constant throughout the reaction. The optimum 4-NP:$NaBH_4$ molar ratio was determined by measuring the time to reaction completion for increasing concentrations of $NaBH_4$, keeping both the initial 4-NP concentration and the catalyst concentration constant. The time required to complete the reaction was seen to decrease with increasing $NaBH_4$ concentration up to a certain value. The molar ratio was considered to be optimized at the lowest $NaBH_4$ concentration that afforded the shortest reaction time.

Reduction of 4-Nitroaniline (4-NA). The experiments were typically carried out by mixing a given amount of ce-MoS_2 into an aqueous solution of 4-NA (0.11 mM). Then, a $NaBH_4$ solution (0.11 M) was added rapidly while stirring, so that the final 4-NA:$NaBH_4$ molar ratio was 1:1000. This optimum molar ratio was determined following the same protocol as described above for the reduction of 4-NP. The reaction progress was monitored by measuring the absorbance of the peak located at 382 nm characteristic of 4-NA.

Reduction of Methyl Orange (MO). In a typical experiment a given amount of ce-MoS_2 and MO (0.07 mM) were first mixed. A $NaBH_4$ solution (0.18 M) was added to this mixture while stirring, so that the final MO:$NaBH_4$ molar ratio was 1:2571. This optimum molar ratio was determined similarly to what has been explained above for 4-NP. The reaction progress was monitored by measuring the absorbance of the peak located at 461 nm.

Reduction of $K_3[Fe(CN)_6]$. In a typical reduction experiment a given amount of ce-MoS_2 was mixed with a solution of $K_3[Fe(CN)_6]$ (1.2 mM), and then $NaBH_4$ solution (0.8 M) was added to trigger the reduction reaction. A $K_3[Fe(CN)_6]$:$NaBH_4$ molar ratio of 1:667, determined to be optimal by the same procedure as described above for the other three model reactions, was used. The reaction progress was monitored by measuring the absorbance of the peak located at 417 nm.

3. RESULTS AND DISCUSSION

Figure 1a (inset, left cuvette) shows a digital photograph of a typical ce-MoS_2 suspension (~0.005 mg mL^{-1}), displaying the grayish tone characteristic of the as-exfoliated material. The

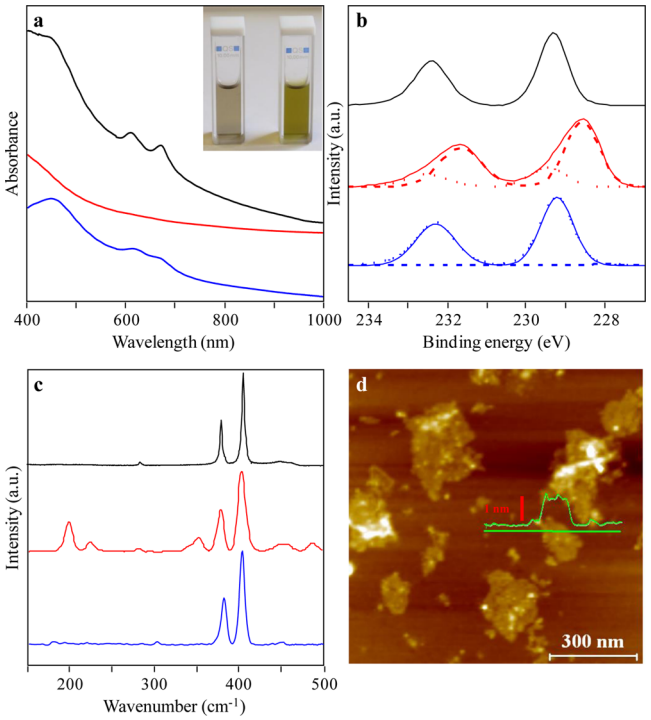

Figure 1. (a) UV−vis absorption spectra of as-prepared ce-MoS_2 dispersion in water (red trace), surfactant (Brij 700)-stabilized aqueous dispersion of MoS_2 obtained by ultrasonication of the starting MoS_2 powder (black trace), and as-prepared ce-MoS_2 suspension after hydrothermal treatment at 200 °C for 4 h (blue trace). Inset: digital photograph of as-prepared (left) and hydrothermally treated (right) ce-MoS_2 dispersion in water at a concentration of 0.005 mg mL^{-1}. (b) High resolution Mo 3d core level XPS spectra of the starting 2H MoS_2 powder (black trace), as-prepared ce-MoS_2 (red trace), and hydrothermally treated ce-MoS_2 (blue trace). (c) Raman spectra of the starting 2H MoS_2 powder (black trace), as-prepared ce-MoS_2 (red trace), and hydrothermally treated ce-MoS_2 (blue trace). (d) AFM image of as-prepared ce-MoS_2 nanosheets cast onto a mica substrate. A typical line profile (green trace) taken along the marked green line is shown overlaid on the image.

UV−vis spectrum of the as-prepared suspension (Figure 1a, red trace) exhibited strong absorbance in the 400−1000 nm wavelength range but was essentially featureless. This is in marked contrast to the case of surfactant-stabilized, multilayer MoS_2 nanosheets prepared by direct ultrasound exfoliation in water, which display distinct absorption bands at ∼400−450, 610, and 670 nm (Figure 1a, black trace).[24,25] The latter type of MoS_2 nanosheet is known to preserve the semiconducting 2H phase of its parent material.[24,25] Thus, the absence of such well-defined absorption bands for as-prepared ce-MoS_2 is an indication of the metallic, 1T character of these nanosheets.[19]

The 1T character of ce-MoS_2 was further corroborated by XPS. The high resolution Mo 3d core level spectrum of 2H MoS_2 (Figure 1b, black trace) shows two peaks located at 229.3 and 232.5 eV, which correspond to the binding energy of Mo^{4+} $3d_{5/2}$ and Mo^{4+} $3d_{3/2}$ levels, respectively, whereas these peaks are downshifted by about 0.7 eV for 1T MoS_2.[19] In agreement with previous reports, each of the two Mo 3d XPS peaks of as-prepared ce-MoS_2 could be fitted to two components associated with the 1T and 2H phases, indicating the simultaneous presence of these two polymorphs (Figure 1b, red trace). Quantification of the fitted components revealed that the 1T phase was clearly dominant in our as-prepared ce-MoS_2 (∼76%) compared to the 2H phase (∼24%). A similar result was obtained from the analysis of S 2p core level spectra (see Supporting Information). It is also worth mentioning that Mo, S, and some residual Li (<1%) were the only elements detected in the survey XPS spectra. The Raman spectrum of 2H MoS_2 (Figure 1c, black trace) is known to be dominated by the well-known E^1_{2g} and A_{1g} bands located at about 380 and 405 cm^{-1},[25] whereas additional peaks at ∼200, 225, and 353 cm^{-1}, associated with the 1T phase, were seen for the as-prepared ce-MoS_2 sample (Figure 1c, red trace).[19,26] AFM imaging revealed that the aqueous ce-MoS_2 dispersions were made up of sheets a few hundred nanometers in lateral size and ∼1 nm of apparent thickness (Figure 1d), consistent with the sheets being single-layer objects.[19,8] Further images of the starting MoS_2 powder and its chemically exfoliated counterpart by FE-SEM can be found in the Supporting Information.

Relevant to the catalytic studies reported below and also to many other potential uses, it was possible to convert the as-prepared aqueous dispersions of 1T ce-MoS_2 back to their 2H counterpart, also in the form of homogeneous dispersion, by hydrothermal treatment of the former in an autoclave at 200 °C. The main requirement to attain a stable suspension was to work at moderate MoS_2 concentrations (e.g., 0.05 mg mL^{-1}). Confirmation of successful recovery of the 2H phase was obtained from UV−vis absorption spectroscopy, XPS, and Raman spectroscopy. The UV−vis spectrum (Figure 1a, blue trace) exhibited well-defined bands at about 400−450, 610, and 670 nm similar to those seen for pristine 2H MoS_2 (Figure 1a, black trace). Further indication of the recovery of the 2H phase was the development of a greenish tone in the suspension (see inset to Figure 1a, right cuvette). Contrary to the case of as-prepared ce-MoS_2, the Mo 3d core level spectrum of the hydrothermally treated sample (Figure 1b, blue trace) was dominated by 2H-related components (fraction of 2H phase greater than 97%). Similarly, the peaks associated with the 1T phase disappeared from the Raman spectrum of hydrothermally treated ce-MoS_2 (Figure 1c, blue trace). Only those characteristic of the 2H polymorph (E^1_{2g} and A_{1g}) were retained.

The catalytic performance of ce-MoS_2 nanosheets was evaluated for a number of model reduction reactions in the aqueous phase at room temperature, specifically those of the substrates 4-nitrophenol (4-NP), 4-nitroaniline (4-NA), methyl orange (MO), and $[Fe(CN)_6]^{3-}$, using $NaBH_4$ as a reductant. The progress of these reactions can be readily monitored by UV−vis absorption spectroscopy. In particular, the reduction of 4-NP to 4-aminophenol (4-AP) with $NaBH_4$ is known to be thermodynamically feasible but kinetically hindered by a relatively high activation barrier. Nevertheless, such reaction is efficiently catalyzed by many noble metal nanostructures and is widely adopted as a benchmark test of their catalytic activity.[27,28] The reaction is also a key step, e.g., in the synthesis of analgesic and antipyretic drugs, such as paracetamol. It is therefore a convenient model reaction to compare the catalytic performance of ce-MoS_2 with that of noble metals. In the absence of $NaBH_4$, the UV−vis spectrum of an aqueous 4-NP solution exhibits a strong absorption band at ∼300 nm, which red-shifts to about 400 nm upon addition of $NaBH_4$ as a result of the increase in pH and subsequent deprotonation of 4-NP to give the 4-nitrophenolate anion (Figure 2a). Reduction of this anion with $NaBH_4$ yields the 4-aminophenolate anion, which displays an absorption band at ∼315 nm and no absorbance at 400 nm (Figure 2a). Therefore, measuring the time evolution of absorbance at 400 nm can be used to follow the conversion

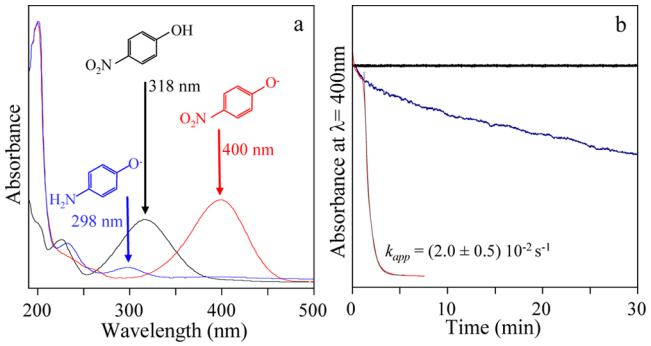

Figure 2. (a) UV−vis absorption spectra aqueous solutions of 4-NP at neutral pH (black trace), under the basic conditions generated in the presence of $NaBH_4$ (4-nitrophenolate anion, red trace), and after reduction of the latter to the 4-aminophenolate anion (blue trace). (b) Plots of the time evolution of absorbance of 4-nitrophenolate at 400 nm in the presence of only $NaBH_4$ (black trace), in the presence of both $NaBH_4$ and ce-MoS_2 nanosheets (red trace), and in the presence of $NaBH_4$ and hydrothermally treated ce-MoS_2 nanosheets (blue trace). The overlaid gray curve is the result of fitting the experimental curve to an exponential decay function. Reaction conditions: [4-NP] = 0.12 mM, [$NaBH_4$] = 72 mM, [ce-MoS_2] = 89 μM.

of 4-nitrophenolate into 4-aminophenolate anion and thus the reaction kinetics.[27,28]

In the absence of any catalyst, the reduction of 4-nitrophenolate by $NaBH_4$ is extremely slow (Figure 2b, black trace). However, when small amounts of aqueous dispersion of the as-prepared ce-MoS_2 nanosheets were added to the reaction medium, a fast conversion was observed (Figure 2b, red trace), suggesting that the nanosheets are able to catalyze the reaction. In the experiments, an excess amount of $NaBH_4$ was used so that its concentration could be considered to remain constant throughout the reaction. In particular, for an initial 4-NP concentration of 0.12 mM the $NaBH_4$ concentration employed was 72 mM, i.e., the 4-NP:$NaBH_4$ molar ratio was 1:600. This particular ratio was determined by measuring the time to reaction completion for increasing concentrations of $NaBH_4$ and selecting the minimum concentration that yielded the shortest reaction time. Under such conditions, the reduction reaction was observed to follow a pseudo-first-order kinetic behavior with respect to 4-NP; i.e., it obeyed the equation

$$\mathrm{d[4\text{-}NP]}/\mathrm{d}t = -k_{\mathrm{app}}[\mathrm{4\text{-}NP}] \quad (1)$$

where [4-NP] is the concentration of 4-NP and k_{app} is the apparent reaction rate constant. The applicability of eq 1 to the present case was demonstrated by the fact that the time evolution of absorbance measured at 400 nm, which reflects the concentration of 4-NP, could be well fitted to an exponential decay function (e.g., see gray curve as a fit to the red trace in Figure 2b). Typical k_{app} values obtained for the reduction of 4-NP were of the order of 10^{-2} s^{-1} (see Figure 2b and below).

A relevant point that needs to be elucidated is whether the catalytic activity observed upon addition of the aqueous ce-MoS_2 suspension is actually originated from the ce-MoS_2 nanosheets themselves or rather from some other component that was present in the aqueous suspension but passed unnoticed. The latter could be some molecular species or minute particles that might have been generated as a byproduct in the preparation of the exfoliated nanosheets or as a result of leaching processes experienced by the nanosheets in the aqueous phase. To address this question, we separated the ce-MoS_2 nanosheets from their aqueous phase by sedimentation using an ultracentrifuge. Were molecular species or tiny nanoparticles the main cause of the observed catalytic behavior, we would expect them to have been largely retained in the resulting supernatant, and hence catalytic activity should also be observed when using such supernatants devoid of ce-MoS_2 nanosheets. However, this was not the case: no reduction at all of 4-NP was seen when using this supernatant and a fast reaction could be attained only in the presence of the nanosheets. Furthermore, if leaching from the nanosheets was

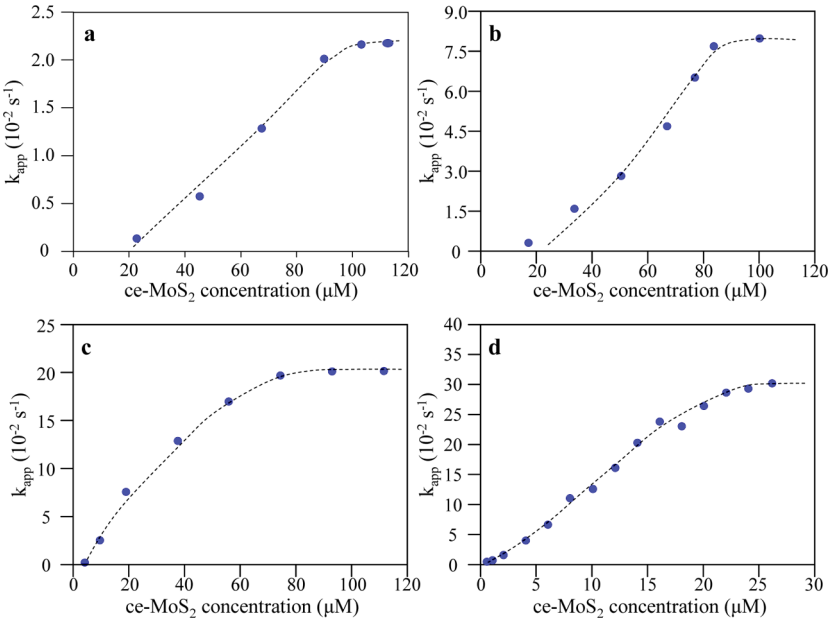

Figure 3. Plots of measured k_{app} values for the reduction of 4- NP (a), 4-NA (b), MO (c), and $[Fe(CN)_6]^{3-}$ (d) with $NaBH_4$ as a function of ce-MoS_2 concentration. Experimental conditions: (a) [4-NP] = 0.12 mM, [$NaBH_4$] = 72 mM, (b) [4-NA] = 0.11 mM, [$NaBH_4$] = 0.11 M, (c) [MO] = 0.07 mM, [$NaBH_4$] = 0.18 M, (d) [$[Fe(CN)_6]^{3-}$] = 1.2 mM, [$NaBH_4$] = 0.8 M.

mostly responsible for the observed catalytic activity, we would expect such activity to increase for aged ce-MoS_2 suspensions compared to the just prepared ones, because the concentration of leached species should increase steadily with time upon preparation and storage of the suspension. Nevertheless, the catalytic activity of aged (several weeks) dispersions was not seen to differ significantly from that of their just prepared counterpart (in the cases of both the whole dispersion and the supernatant after removal of the nanosheets), suggesting that leaching processes are not relevant in the present case. The fact that the ce-MoS_2 nanosheets were well dispersed in water, thereby maximizing their surface area directly exposed to the aqueous medium, was also instrumental in attaining a high catalytic activity. When agglomeration of the nanosheets was induced by the addition of an electrolyte (e.g., NaCl) to the aqueous dispersion, the catalytic activity was seen to decrease very significantly.

Figure 3 plots the value of k_{app} measured for each of the reduction reactions under investigation and for different concentrations of ce-MoS_2 nanosheets in the reaction medium. As could be anticipated, the catalytic activity tended to increase with nanosheet concentration until a saturation point was reached. This saturation point sets the optimum catalyst concentration, which under the present experimental conditions could be estimated at about 90 μM, 77 μM, 74 μM, and 22 μM for 4-NP, 4-NA, MO, and $[Fe(CN)_6]^{3-}$, respectively. Likewise, having established that the observed catalytic activity is due to the ce-MoS_2 nanosheets, the question arises as to which features of the nanosheets confer them such activity. Here, we show that the presence of the 1T phase in the nanosheets is mostly responsible for their catalytic behavior. Figure 2b compares the catalytic activity, in terms of time evolution of the absorption peak at 400 nm of the 4-nitrophenolate anion, of the as-prepared 1T-dominated ce-MoS_2 nanosheets (red trace) with that of the same nanosheets after their conversion back to the 2H phase by means of hydrothermal treatment as described above (blue trace). The reduction of 4-nitrophenolate was much faster using 1T ce-MoS_2, suggesting that transformation of the thermodynamically stable, semiconducting 2H polymorph of MoS_2 into the metastable metallic 1T phase is required to activate the nanosheets toward this catalytic reaction. The catalytic activity of the 2H ce-MoS_2 nanosheets was seen to be very low, but non-negligible (k_{app} of the order of 10^{-4} s^{-1}). This can be due either to the presence of some remnant 1T phase in the nanosheets that could not be fully removed by the hydrothermal treatment, as noted beforehand, or to the catalytic activity that is generally associated with metallic edges of 2H MoS_2.[12,15] Being of relatively limited lateral dimensions (typically below 0.5 μm; see Figure 1d), the present nanosheets should exhibit a small but non-negligible fraction of edges in their structure, which could contribute to their catalytic activity.

Another relevant issue that should be addressed when reporting the performance of a catalyst is to establish comparisons between its activity and that of other efficient catalysts for the same reaction. Several noble metals (Au, Ag, Pt, Pd) in nanoparticulate form are known to be markedly active catalysts in the reduction of 4-NP by $NaBH_4$.[27,28] Here, comparisons between different catalysts have been made on the basis of their turnover frequency (TOF), which is defined as the number of moles of substrate (4-NP) converted per mole of catalyst per minute. Table 1 lists TOF values for the present ce-MoS_2 nanosheets and a representative set of state-of-the-art noble metal catalysts that have been reported in the literature for the reduction of 4-NP.[29−43] We note that for the calculation of TOF values we chose to use the total number of moles of ce-MoS_2 present in the reaction medium, rather than the number of moles of catalytically active sites on the sheets, which was unknown. This is similar to what is commonly done in catalytic studies of 4-NP reduction with noble metal nanoparticles, so that the comparisons given in Table 1 are all made on an equal footing. The TOF value of 1T ce-MoS_2 nanosheets was determined to be 0.74 min^{-1}, which is comparable to that of many catalysts based on noble metals, indicating that the former are also efficient for this reaction. Although not inactive as a catalyst, this is, however, not the case of 2H ce-MoS_2 nanosheets (TOF ~ 0.015 min^{-1}), which stresses the idea that phase transformation of 2H to 1T MoS_2 is highly desirable to trigger its catalytic performance. We also note that some noble metal catalysts (e.g., Pd nanoparticles supported onto functionalized carbon nanotubes; see Table 1) displayed considerably larger TOF values than those of 1T ce-MoS_2 and other noble metal-based catalysts. However, they are based on scarce and expensive elements and often make use of sophisticated supports and/or preparation procedures. By contrast, the present ce-MoS_2 nanosheets combine the fact that they are based on more earth-abundant elements, a relative simplicity of preparation, and a competitive catalytic activity, thereby constituting an attractive alternative to noble metal-based catalysts. Another 2D material that has been postulated as a cost-effective alternative to noble metal catalysts toward several oxidation, reduction, and other reactions is certain types of graphene-based nanosheets, in particular those derived from graphene oxide (GO).[44] More specifically, reduced GO as well as reduced and nitrogen-doped GO nanosheets prepared

Table 1. Comparison of Turnover Frequency (TOF) Values for the Reduction of 4-NP with $NaBH_4$ Using Different Catalysts

catalyst	TOF (min^{-1})	ref
1T ce-MoS_2 nanosheets	0.74	present work
2H ce-MoS_2 nanosheets	0.015	present work
5 nm-sized citrate-capped Au NPs	1.4	29
Au NPs deposited onto PMMA	1.5	30
Au NPs on ionic liquid-modified silica	19.1	31
Au NP/graphene hydrogel	0.19	32
hollow Ag nanospheres	0.16	33
Ag NP−chitosan composite	0.1	34
Ag NPs on carbon nanofibers	0.58	35
Ag NPs on alginate microspheres	1.9	36
surfactant-capped Pt nanocubes	2.5	37
Pt NPs derived from wood nanomaterials	0.03−0.26	38
Pd NPs in graphene@carbon hollow spheres	4.56	39
Pd NPs on covalently funcionalized CNTs	18	40
Pd NPs supported onto CNTs	6.3	41
Pentacle Au−Cu alloy nanocrystals	0.8−1.7	29
Pt−Au alloy NPs on carbon derived from IL	0.2	42
Au−Pd alloy nanodendrites	0.4	43
hydrothermally reduced GO nanosheets	$0.8-2.8 \times 10^{-3}$	21 and present work
N-doped reduced GO nanosheets	$0.7-1 \times 10^{-3}$	23 and present work

through hydrothermal methods have very recently been shown to exhibit catalytic activity in the reduction of 4-NP.[21,23] It was thus pertinent to compare the performance of all these 2D materials devoid of noble metals (i.e., 1T ce-MoS_2, 2H ce-MoS_2, reduced GO, and reduced and nitrogen-doped GO) as catalysts. To this end, we prepared both types of GO nanosheet and investigated their catalytic activity toward reduction of 4-NP. The results indicate that the materials derived from GO possess a rather low catalytic activity (TOF values of the order of 10^{-3} min^{-1}, see Table 1) compared to that of both 1T ce-MoS_2 and noble metal-based catalysts. We note that the lithium intercalation reaction of the MoS_2 powder was accomplished at room temperature. However, carrying out this reaction at higher temperatures might improve the degree of lithium intercalation of the material and, consequently, its extent of conversion to the 1T phase and the catalytic activity of the resulting ce-MoS_2 nanosheets. Nevertheless, the conversion of 2H to 1T phase in the present work was quite high (~76%; see above). In fact, it was higher than that attained in previous reports using the same intercalation conditions, which is typically around 50%.[19] We believe that this could be due to a smaller particle size of our starting MoS_2 powder, as this parameter is generally known to be relevant in the efficiency of intercalation reactions. Consequently, although there is still some room for improvement in the extent of conversion of the material to the metallic 1T phase and hence probably in the catalytic activity of the ce-MoS_2 nanosheets, most of the beneficial effect of the 1T polymorph should have already been attained here. Anyhow, care should also be exercised when pursuing higher conversion degrees to the 1T polymorph by performing the intercalation reaction at higher temperatures or, e.g., by using larger amounts of *n*-butyllithium. In this case, there is the risk of decomposition of the MoS_2 host to yield unwanted products such as Li_2S and Mo.[8]

The scope of 1T ce-MoS_2 nanosheets as an efficient catalyst in reduction reactions by $NaBH_4$ was not limited to 4-NP. As has been mentioned, other substrates were tested, i.e., 4-NA, MO, and $[Fe(CN)_6]^{3-}$, all of which could be successfully reduced in the presence of the nanosheets. Typical k_{app} values for these reactions were in the 10^{-2}–10^{-1} s^{-1} range (see Figure 3 and Supporting Information for further details). Again, their catalytic performance, expressed in terms of TOF values, was comparable to that obtained using noble metal nanoparticles (see Table 2),[33,45−51] further highlighting the efficiency of 1T ce-MoS_2 as a catalyst. The reusability of the catalyst was also tested by repeating the reduction reaction several times, adding sequentially a given amount of substrate to the colloidal suspension of ce-MoS_2 containing an excess amount of $NaBH_4$. This is exemplified in Figure 4 for the case of $[Fe(CN)_6]^{3-}$, which indicated that the k_{app} value increases in the second reaction cycle and then moderately decreases over the next cycles, so that k_{app} in the 10th cycle is essentially the same as that of the first one. This result indicates that the catalytic activity of the nanosheets is mostly preserved upon consecutive reaction cycles.

Next, the possible mechanism that allows reduction of 4-NP and the other reagents by $NaBH_4$, as mediated by the ce-MoS_2 nanosheets, is briefly discussed. In the case of some noble metal (e.g., Au) nanoparticles, the BH_4^- anion has been shown to inject electrons to the nanoparticles, which thereby become a reservoir of excess electrons.[27] The latter are then readily transferred to the substrate molecules (e.g., 4-NP) upon their adsorption onto the nanoparticles, thus triggering their

Table 2. Comparison of TOF Values for Different Catalysts in the Reduction of 4-NA, MO, and $[Fe(CN)_6]^{3-}$

catalyst	TOF (min^{-1})	ref
Reduction of 4-NA		
1T ce-MoS_2 nanosheets	1.39 ± 0.08	present work
N-doped reduced GO nanosheets	1.4×10^{-3}	present work
hollow Ag nanospheres	0.10	33
rhombic dodecahedral Au NPs	0.10	45
cubic Au NPs	0.08	45
octahedral Au NPs	0.02	45
Au NPs embedded in hydrogel matrix	0.49	46
Au NW networks	0.06–0.18	47
Reduction of MO		
1T ce-MoS_2 nanosheets	2.5 ± 0.4	present work
Au or Ag NPs on dendrimer-grafted GO	~10^{-3}	48
Ag NPs	0.6	49
Au NPs	0.05	49
Pt NPs	0.04	49
Pt nanocubes on ITO substrate	1.7	50
Reduction of $[Fe(CN)_6]^{3-}$		
1T ce-MoS_2 nanosheets	392 ± 32	present work
Au NPs embedded in polymer microgel	0.1	51

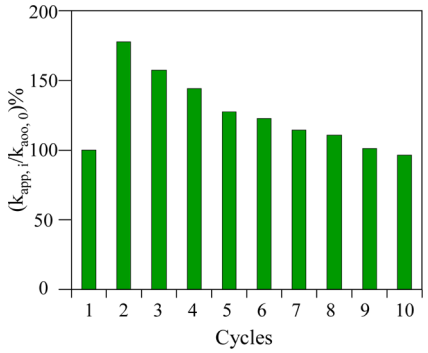

Figure 4. Reusability experiments of ce-MoS_2 nanosheets in the catalytic reduction of $[Fe(CN)_6]^{3-}$. $NaBH_4$ was only added in the first catalytic cycle ($[NaBH_4]$ = 0.16 M), and the same amount of $[Fe(CN)_6]^{3-}$ (1.2 mM) was added in each consecutive cycle. [ce-MoS_2] = 22 μM.

reduction. However, we believe that direct injection of electrons from the BH_4^- anion to the ce-MoS_2 nanosheets is not the main pathway that affords reduction of 4-NP and the other substrate molecules in the presence of the nanosheets. For the mentioned noble metal nanoparticles, this catalytic process is insensitive to the pH of the aqueous medium, and in particular it is insensitive to high pH values.[52] On the other hand, we observed that the catalytic activity of the ce-MoS_2 nanosheets became arrested at pH values above ~11, i.e., no reduction of 4-NP and the other molecules was attained under basic conditions. We note that at pH values up to about 11, the BH_4^- anion hydrolyzes spontaneously at a slow but non-negligible rate in aqueous medium, whereas hydrolysis becomes arrested at higher pH,[53,54] suggesting that some product of the hydrolysis of the BH_4^- anion, rather than BH_4^- itself, is directly involved in the reduction reactions catalyzed by ce-MoS_2.

The spontaneous hydrolysis of BH_4^- is known to proceed according to the following equation:[54−56]

$$BH_4^- + H_2O \rightarrow BH_3OH^- + H_2 \quad (2)$$

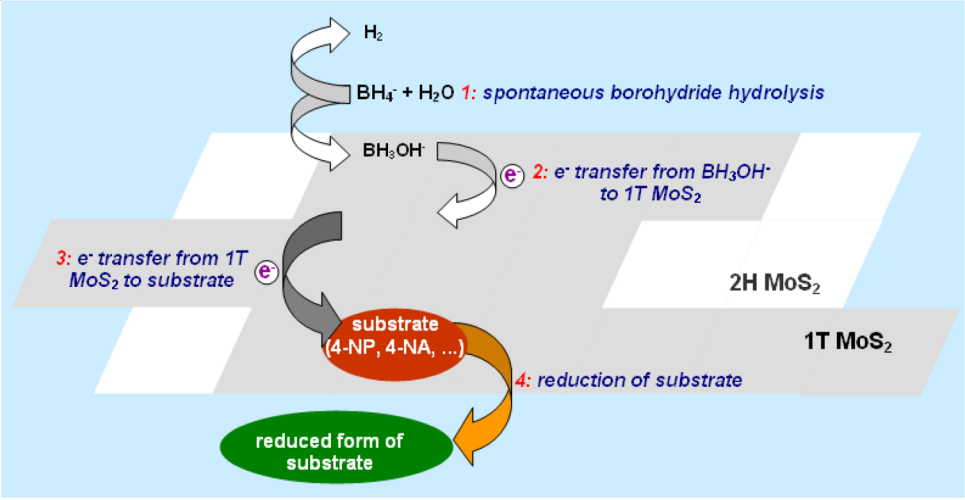

Figure 5. Schematic of the overall mechanistic pathway for reduction reactions catalyzed by ce-MoS_2 nanosheets with $NaBH_4$ in aqueous medium. The BH_4^- anion hydrolyzes spontaneously in water to give H_2 and the BH_3OH^- anion (1), and then the latter species injects electrons to metallic 1T sites of ce-MoS_2 (2), which are finally transferred to the substrate molecule (4-NP, 4-NA, etc.) (3) to trigger its reduction (4).

where the BH_3OH^- anion is an intermediate but relatively stable product that is further hydrolyzed as follows

$$BH_3OH^- + H_2O \rightarrow BO_2^- + 3H_2 \quad (3)$$

Equations 2 and 3 indicate that there are three potential candidates for the compound directly involved in the reduction reactions catalyzed by ce-MoS_2. In principle, the most obvious one would be H_2. However, control experiments in which a H_2 flow was passed through a 4-NP solution in the presence of ce-MoS_2 nanosheets did not succeed in reducing the substrate, even if the gas flow was several orders of magnitude larger than the hydrolysis rate of BH_4^-. This result points to the idea that H_2 cannot be dissociated on the ce-MoS_2 nanosheets, at least at room temperature. The metaborate anion (BO_2^-) was not found to be responsible for the reported reduction reactions, because no reductions could be attained by substituting $NaBO_2$ for $NaBH_4$ in the reaction medium. Hence, the BH_3OH^- anion is suggested to be the actual reductant for the reactions catalyzed by ce-MoS_2. Such a scenario would thus be similar to that recently found to be in place for some reduction reactions catalyzed by Ag nanoparticles using $NaBH_4$. For this particular noble metal, the BH_3OH^- anion, and not BH_4^-, is the species that injects excess electrons to the nanoparticle, which are then used to promote reduction reactions.[57] Consequently, we propose the overall mechanistic pathway for the reduction reactions catalyzed by ce-MoS_2 nanosheets that is schematically depicted in Figure 5.

A last point that should be commented upon concerns the specific characteristics of ce-MoS_2 that confer the nanosheets the reported catalytic activity. As discussed above, only nanosheets with a significant fraction of metallic 1T phase were effective catalysts, whereas the same nanosheets after conversion back to the semiconducting 2H polymorph performed poorly in comparison. It could thus be postulated that the transfer of electrons from the reductant to the substrate molecule (4-NP, 4-NA, etc.) would be facilitated by the metallic nature of the 1T phase compared to the semiconducting character of its 2H counterpart. However, we note that the structure of ce-MoS_2 has been previously shown not to be purely 1T but distorted (strained) 1T.[58,59] Furthermore, recent work has demonstrated that the concurrent presence of strain and metallic 1T sites in chemically exfoliated WS_2 nanosheets was the decisive factor for the enhanced catalytic activity of these nanosheets toward the HER.[60,61] A similar combined effect might also be responsible for the high catalytic activity of ce-MoS_2 toward the reduction reactions reported here, but elucidating this question will most probably require resorting to theoretical calculations. Similar TMD materials dominated by the 1T phase (e.g., WS_2) are also expected to exhibit catalytic activity for the same type of reactions documented here. Indication for this is obtained from a very recent report indicating that W@WS_2 nanorattles with 2H phase but exhibiting a relatively large fraction of edges are catalytically active in similar reactions to those studied here (reduction of 2-nitroaniline with $NaBH_4$).[62]

4. CONCLUSIONS

In conclusion, we have demonstrated that chemically exfoliated MoS_2 nanosheets with a dominant contribution of the metallic 1T phase exhibit a high catalytic activity toward reduction reactions at room temperature in aqueous medium using $NaBH_4$ as a reductant. The performance of the nanosheets was seen to be comparable to that of many noble metal-based catalysts, thus establishing such two-dimensional material as a potential inexpensive, earth-abundant alternative to the latter in catalysis beyond the hydrogen evolution reaction. Further studies on the catalytic activity of chemically exfoliated nanosheets of MoS_2 and other transition metal dichalcogenides toward a number of other reactions can be expected to follow.

■ ASSOCIATED CONTENT

Supporting Information

XPS spectra of MoS_2 samples, FE-SEM images, and kinetic profiles for reduction reactions. This material is available free of charge via the Internet at http://pubs.acs.org.

■ AUTHOR INFORMATION

Corresponding Author

*Telephone: (+34) 985 11 90 90. Fax: (+34) 985 29 76 62. E-mail: lauraguardia@incar.csic.es (L. Guardia).

Notes

The authors declare no competing financial interest.

■ ACKNOWLEDGMENTS

Financial support from the Spanish MINECO and the European Regional Development Fund through Project MAT2011-26399 is gratefully acknowledged. M.A.-V. is thankful for the receipt of a predoctoral contract (FPI) from MINECO.

■ REFERENCES

(1) Lancaster, M. *Green Chemistry: An Introductory Text*; RSC Publishing: Cambridge, 2010; Chapter 4, pp 90−138.
(2) Kobayashi, S.; Yamashita, Y. Alkaline Earth Metal Catalysts for Asymmetric Reactions. *Acc. Chem. Res.* **2011**, *44*, 58−71.
(3) Du, P.; Eisenberg, R. Catalysts Made of Earth-Abundant Elements (Co, Ni, Fe) for Water Splitting: Recent Progress and Future Challenges. *Energy Environ. Sci.* **2012**, *5*, 6012−6021.
(4) McKone, J. R.; Marinescu, S. C.; Brunschwig, B. S.; Winkler, J. R.; Gray, H. B. Earth-Abundant Hydrogen Evolution Electrocatalysts. *Chem. Sci.* **2014**, *5*, 865−878.
(5) Faber, M. S.; Jin, S. Earth-Abundant Inorganic Electrocatalysts and their Nanostructures for Energy Conversion Applications. *Energy Environ. Sci.* **2014**, *7*, 3519−3542.
(6) Xu, M.; Liang, T.; Shi, M.; Chen, H. Graphene-Like Two-Dimensional Materials. *Chem. Rev.* **2013**, *113*, 3766−3798.
(7) Butler, S. Z.; Hollen, S. M.; Cao, L.; Cui, Y.; Gupta, J. A.; Gutiérrez, H. R.; Heinz, T. F.; Hong, S. S.; Huang, J.; Ismach, A. F.; Johnston-Halperin, E.; Kuno, M.; Plashnitsa, V. V.; Robinson, R. D.; Ruoff, R. S.; Salahuddin, S.; Shan, J.; Shi, L.; Spencer, M. G.; Terrones, M.; Windl, W.; Goldberger, J. E. Progress, Challenges, and Opportunities in Two-Dimensional Materials Beyond Graphene. *ACS Nano* **2013**, *7*, 2898−2926.
(8) Chhowalla, M.; Shin, H. S.; Eda, G.; Li, L.-J.; Loh, K. P.; Zhang, H. The Chemistry of Two-Dimensional Layered Transition Metal Dichalcogenide Nanosheets. *Nat. Chem.* **2013**, *5*, 263−275.
(9) Quinn, M. D. J.; Ho, N. H.; Notley, S. M. Aqueous Dispersions of Exfoliated Molybdenum Disulfide for Use in Visible-Light Photocatalysis. *ACS Appl. Mater. Interfaces* **2013**, *5*, 12751−12756.
(10) Nicolosi, V.; Chhowalla, M.; Kanatzidis, M. G.; Strano, M. S.; Coleman, J. N. Liquid Exfoliation of Layered Materials. *Science* **2013**, *340*, 1226419.
(11) Song, F.; Hu, X. Exfoliation of Layered Double Hydroxides for Enhanced Oxygen Evolution Catalysis. *Nat. Commun.* **2014**, *5*, 4477.
(12) Chianelli, R. R.; Siadati, M. H.; Perez De la Rosa, M.; Berhault, G.; Wilcoxon, J. P.; Bearden, R., Jr.; Abrams, B. L. Catalytic Properties of Single Layers of Transition Metal Sulfide Catalytic Materials. *Catal. Rev.* **2006**, *48*, 1−41.
(13) Hinnemann, B.; Moses, P. G.; Bonde, J.; Jørgensen, K. P.; Nielsen, J. H.; Horch, S.; Chorkendorff, I.; Nørskov, J. K. Biomimetic Hydrogen Evolution: MoS_2 Nanoparticles as Catalyst for Hydrogen Evolution. *J. Am. Chem. Soc.* **2005**, *127*, 5308−5309.
(14) Jaramillo, T. F.; Jørgensen, K. P.; Bonde, J.; Nielsen, J. H.; Horch, S.; Chorkendorff, I. Identification of Active Edge Sites for Electrochemical H_2 Evolution from MoS_2 Nanocatalysts. *Science* **2007**, *317*, 100−102.
(15) Laursen, A. B.; Kegnæs, S.; Dahla, S.; Chorkendorff, I. Molybdenum Sulfides-Efficient and Viable Materials for Electro- and Photoelectrocatalytic Hydrogen Evolution. *Energy Environ. Sci.* **2012**, *5*, 5577−5591.
(16) Lukowski, M. A.; Daniel, A. S.; Meng, F.; Forticaux, A.; Li, L.; Jin, S. Enhanced Hydrogen Evolution Catalysis from Chemically Exfoliated Metallic MoS_2 Nanosheets. *J. Am. Chem. Soc.* **2013**, *135*, 10274−10277.
(17) Voiry, D.; Salehi, M.; Silva, R.; Fujita, T.; Chen, M.; Asefa, T.; Shenoy, V. B.; Eda, G.; Chhowalla, M. Conducting MoS_2 Nanosheets as Catalysts for Hydrogen Evolution Reaction. *Nano Lett.* **2013**, *13*, 6222−6227.
(18) Joensen, P.; Frindt, R. F.; Morrison, S. R. Single-layer MoS_2. *Mater. Res. Bull.* **1986**, *21*, 457−461.
(19) Eda, G.; Yamaguchi, H.; Voiry, D.; Fujita, T.; Chen, M.; Chhowalla, M. Photoluminescence from Chemically Exfoliated MoS_2. *Nano Lett.* **2011**, *11*, 5111−5116.
(20) Paredes, J. I.; Villar-Rodil, S.; Solís-Fernández, P.; Martínez-Alonso, A.; Tascón, J. M. D. Atomic Force and Scanning Tunneling Microscopy Imaging of Graphene Nanosheets Derived from Graphite Oxide. *Langmuir* **2009**, *25*, 5957−5968.
(21) Kong, X.-K.; Chen, Q.-W.; Lun, Z.-Y. Probing the Influence of Different Oxygenated Groups on Graphene Oxide's Catalytic Performance. *J. Mater. Chem. A* **2014**, *2*, 610−613.
(22) Nethravathi, C.; Rajamathi, M. Chemically Modified Graphene Sheets Produced by the Solvothermal Reduction of Colloidal Dispersions of Graphite Oxide. *Carbon* **2008**, *46*, 1994−1998.
(23) Kong, X.-K.; Sun, Z.-Y.; Chen, M.; Chen, C.-L.; Chen, Q.-W. Metal-Free Catalytic Reduction of 4-Nitrophenol to 4-Aminophenol by N-Doped Graphene. *Energy Environ. Sci.* **2013**, *6*, 3260−3266.
(24) Smith, R. J.; King, P. J.; Lotya, M.; Wirtz, C.; Khan, U.; De, S.; O'Neill, A.; Duesberg, G. S.; Grunlan, J. C.; Moriarty, G.; Chen, J.; Wang, J.; Minett, A. I.; Nicolosi, V.; Coleman, J. N. Large-Scale Exfoliation of Inorganic Layered Compounds in Aqueous Surfactant Solutions. *Adv. Mater.* **2011**, *23*, 3944−3948.
(25) Guardia, L.; Paredes, J. I.; Rozada, R.; Villar-Rodil, S.; Martínez-Alonso, A.; Tascón, J. M. D. Production of Aqueous Dispersions of Inorganic Graphene Analogues by Exfoliation and Stabilization with Non-Ionic Surfactants. *RSC Adv.* **2014**, *4*, 14115−14127.
(26) Zheng, J.; Zhang, H.; Dong, S.; Liu, Y.; Nai, C. T.; Shin, H. S.; Jeong, H. Y.; Liu, B.; Loh, K. P. High Yield Exfoliation of Two-Dimensional Chalcogenides using Sodium Naphthalenide. *Nat. Commun.* **2014**, *5*, 2995.
(27) Hervés, P.; Pérez-Lorenzo, M.; Liz-Marzán, L. M.; Dzubiella, J.; Lubc, Y.; Ballauff, M. Catalysis by Metallic Nanoparticles in Aqueous Solution: Model Reactions. *Chem. Soc. Rev.* **2012**, *41*, 5577−5587.
(28) Fernández-Merino, M. J.; Villar-Rodil, S.; Paredes, J. I.; Solís-Fernández, P.; Guardia, L.; García, R.; Martínez-Alonso, A.; Tascón, J. M. D. Identifying Efficient Natural Bioreductants for the Preparation of Graphene and Graphene-Metal Nanoparticle Hybrids with Enhanced Catalytic Activity from Graphite Oxide. *Carbon* **2013**, *63*, 30−44.
(29) He, R.; Wang, Y.-C.; Wang, X.; Wang, Z.; Liu, G.; Zhou, W.; Wen, L.; Li, Q.; Wang, X.; Chen, X.; Zeng, J.; Hou, J. G. Facile Synthesis of Pentacle Gold−Copper Alloy Nanocrystals and their Plasmonic and Catalytic Properties. *Nat. Commun.* **2014**, *5*, 4327.
(30) Kuroda, K.; Ishida, T.; Haruta, M. Reduction of 4-Nitrophenol to 4-Aminophenol over Au Nanoparticles Deposited on PMMA. *J. Mol. Catal. A: Chem.* **2009**, *298*, 7−11.
(31) Yang, H.; Li, S.; Zhang, X.; Wang, X.; Ma, J. Imidazolium Ionic Liquid-Modified Fibrous Silica Microspheres Loaded with Gold Nanoparticles and their Enhanced Catalytic Activity and Reusability for the Reduction of 4-Nitrophenol. *J. Mater. Chem. A* **2014**, *2*, 12060−12067.
(32) Li, J.; Liu, C.-Y.; Liu, Y. Au/Graphene Hydrogel: Synthesis, Characterization and its Use for Catalytic Reduction of 4-Nitrophenol. *J. Mater. Chem.* **2012**, *22*, 8426−8430.
(33) Vadakkekara, R.; Chakraborty, M.; Parikh, P. A. Reduction of Aromatic Nitro Compounds on Colloidal Hollow Silver Nanospheres. *Colloids Surf., A* **2012**, *399*, 11−17.
(34) Murugadoss, A.; Chattopadhyay, A. A "Green" Chitosan−Silver Nanoparticle Composite as a Heterogeneous as well as Micro-Heterogeneous Catalyst. *Nanotechnology* **2008**, *19*, 015603.
(35) Zhang, P.; Shao, C.; Zhang, Z.; Zhang, M.; Mu, J.; Guo, Z.; Liu, Y. In Situ Assembly of Well-Dispersed Ag Nanoparticles (AgNPs) on Electrospun Carbon Nanofibers (CNFs) for Catalytic Reduction of 4-Nitrophenol. *Nanoscale* **2011**, *3*, 3357−3363.
(36) You, J.; Zhao, C.; Cao, J.; Zhou, J.; Zhang, L. Fabrication of High-Density Silver Nanoparticles on the Surface of Alginate Microspheres for Application in Catalytic Reaction. *J. Mater. Chem. A* **2014**, *2*, 8491−8499.

(37) Kim, C.; Lee, H. Change in the Catalytic Reactivity of Pt Nanocubes in the Presence of Different Surface-Capping Agents. *Catal. Commun.* **2009**, *10*, 1305−1309.
(38) Lin, X.; Wu, M.; Wu, D.; Kuga, S.; Endo, T.; Huang, Y. Platinum Nanoparticles using Wood Nanomaterials: Eco-Friendly Synthesis, Shape Control and Catalytic Activity for p-Nitrophenol Reduction. *Green Chem.* **2011**, *13*, 283−287.
(39) Zhang, Z.; Xiao, F.; Xi, J.; Sun, T.; Xiao, S.; Wang, H.; Wang, S.; Liu, Y. Encapsulating Pd Nanoparticles in Double-Shelled Graphene@ Carbon Hollow Spheres for Excellent Chemical Catalytic Property. *Sci. Rep.* **2014**, *4*, 4053.
(40) Gu, X.; Qi, W.; Xu, X.; Sun, Z.; Zhang, L.; Liu, W.; Panb, X.; Su, D. Covalently Functionalized Carbon Nanotube Supported Pd Nanoparticles for Catalytic Reduction of 4-Nitrophenol. *Nanoscale* **2014**, *6*, 6609−6616.
(41) Li, H.; Han, L.; Cooper-White, J.; Kimc, I. Palladium Nanoparticles Decorated Carbon Nanotubes: Facile Synthesis and their Applications as Highly Efficient Catalysts for the Reduction of 4-Nitrophenol. *Green Chem.* **2012**, *14*, 586−591.
(42) Peng, Y.; Wu, X.; Qiu, L.; Liu, C.; Wang, S.; Yan, F. Synthesis of Carbon−PtAu Nanoparticle Hybrids Originating from Triethoxysilane-Derivatized Ionic Liquids for Methanol Electrooxidation and the Catalytic Reduction of 4-Nitrophenol. *J. Mater. Chem. A* **2013**, *1*, 9257−9263.
(43) Shi, L.; Wang, A.; Zhang, T.; Zhang, B.; Su, D.; Li, H.; Song, Y. One-Step Synthesis of Au−Pd Alloy Nanodendrites and their Catalytic Activity. *J. Phys. Chem. C* **2013**, *117*, 12526−12536.
(44) Navalon, S.; Dhakshinamoorthy, A.; Alvaro, M.; Garcia, H. Carbocatalysis by Graphene-Based Materials. *Chem. Rev.* **2014**, *114*, 6179−6212.
(45) Chiu, C.-Y.; Chung, P.-J.; Lao, K.-U.; Liao, C.-W.; Huang, M. H. Facet-Dependent Catalytic Activity of Gold Nanocubes, Octahedra, and Rhombic Dodecahedra toward 4-Nitroaniline Reduction. *J. Phys. Chem. C* **2012**, *116*, 23757−23763.
(46) Ramtenki, V.; Anumon, V. D.; Badiger, M. V.; Prasad, B. L. V. Gold Nanoparticle Embedded Hydrogel Matrices as Catalysts: Better Dispersibility of Nanoparticles in the Gel Matrix upon Addition of N-Bromosuccinimide Leading to Increased Catalytic Efficiency. *Colloids Surf., A* **2012**, *414*, 296−301.
(47) Chirea, M.; Freitas, A.; Vasile, B. S.; Ghitulica, C.; Pereira, C. M.; Silva, F. Gold Nanowire Networks: Synthesis, Characterization, and Catalytic Activity. *Langmuir* **2011**, *27*, 3906−3913.
(48) Rajesh, R.; Kumarb, S. S.; Venkatesan, R. Efficient Degradation of Azo Dyes Using Ag and Au Nanoparticles Stabilized on Graphene Oxide Functionalized with PAMAM Dendrimers. *New J. Chem.* **2014**, *38*, 1551−1558.
(49) Gupta, N.; Singh, H. P.; Sharma, R. K. Metal Nanoparticles with High Catalytic Activity in Degradation of Methyl Orange: An Electron Relay Effect. *J. Mol. Catal. A: Chem.* **2011**, *335*, 248−252.
(50) Balouch, A.; Umar, A. A.; Tan, S. T.; Nafisah, S.; Saad, S. K. M.; Salleha, M. M.; Oyamac, M. Fibrous, Ultra-Small Nanorod-Constructed Platinum Nanocubes Directly Grown on the ITO Substrate and their Heterogeneous Catalysis Application. *RSC Adv.* **2013**, *3*, 19789−19792.
(51) Xiao, C.; Wu, Q.; Chang, A.; Peng, Y.; Xu, W.; Wu, W. Responsive Au@Polymer Hybrid Microgels for the Simultaneous Modulation and Monitoring of Au-Catalyzed Chemical Reaction. *J. Mater. Chem. A* **2014**, *2*, 9514−9523.
(52) Carregal-Romero, S.; Buurma, N. J.; Pérez-Juste, J.; Liz-Marzán, L. M.; Hervés, P. Catalysis by Au@pNIPAM Nanocomposites: Effect of the Cross-Linking Density. *Chem. Mater.* **2010**, *22*, 3051−3059.
(53) Marrero-Alfonso, E. Y.; Beaird, A. M.; Davis, T. A.; Mathews, M. A. Hydrogen Generation from Chemical Hydrides. *Ind. Eng. Chem. Res.* **2009**, *48*, 3703−3712.
(54) Chatenet, M.; Micoud, F.; Roche, I.; Chainet, E. Kinetics of Sodium Borohydride Direct Oxidation and Oxygen Reduction in Sodium Hydroxide Electrolyte: Part I. BH_4^- Electro-Oxidation on Au and Ag Catalysts. *Electrochim. Acta* **2006**, *51*, 5459−5467.
(55) Gardiner, J. A.; Collat, J. W. The Hydrolysis of Sodium Tetrahydroborate. Identification of an Intermediate. *J. Am. Chem. Soc.* **1964**, *86*, 3165−3166.
(56) Andrieux, J.; Demirci, U. B.; Hannauer, J.; Gervais, C.; Goutaudier, C.; Miele, P. Spontaneous Hydrolysis of Sodium Borohydride In Harsh Conditions. *Int. J. Hydrogen Energy* **2011**, *36*, 224−233.
(57) Ayán-Varela, M.; Fernández-Merino, M. J.; Paredes, J. I.; Villar-Rodil, S.; Fernández-Sánchez, C.; Guardia, L.; Martínez-Alonso, A.; Tascón, J. M. D. Highly Efficient Silver-Assisted Reduction of Graphene Oxide Dispersions at Room Temperature: Mechanism, and Catalytic and Electrochemical Performance of the Resulting Hybrids. *J. Mater. Chem. A* **2014**, *2*, 7295−7305.
(58) Yang, D.; Sandoval, S. J.; Divigalpitiya, W. M. R.; Irwin, J. C.; Frindt, R. F. Structure of Single-Molecular-Layer MoS_2. *Phys. Rev. B* **1991**, *43*, 12053−12056.
(59) Heising, J.; Kanatzidis, M. G. Structure of Restacked MoS_2 and WS_2 Elucidated by Electron Crystallography. *J. Am. Chem. Soc.* **1999**, *121*, 638−643.
(60) Voiry, D.; Yamaguchi, H.; Li, J.; Silva, R.; Alves, D. C. B.; Fujita, T.; Chen, M.; Asefa, T.; Shenoy, V. B.; Eda, G.; Chhowalla, M. Enhanced Catalytic Activity in Strained Chemically Exfoliated WS_2 Nanosheets for Hydrogen Evolution. *Nat. Mater.* **2013**, *12*, 850−855.
(61) Lukowski, M. A.; Daniel, A. S.; English, C. R.; Meng, F.; Forticaux, A.; Hamers, R. J.; Jin, S. Highly Active Hydrogen Evolution Catalysis from Metallic WS_2 Nanosheets. *Energy Environ. Sci.* **2014**, *7*, 2608−2613.
(62) Wen, Y.; Zhang, H.; Zhang, S. One-Step Gas−Solid Reaction Synthesis of W@WS_2 Nanorattles and their Novel Catalytic Activity. *Nanoscale* **2014**, *6*, 13090−13096.